Solid State Communications 250 (2017) 35–40

Contents lists available at ScienceDirect

Solid State Communications

journal homepage: www.elsevier.com/locate/ssc

Communication

Comparison of Heine–Abarenkov and alternative pseudopotentials for electron–phonon interaction in aluminium, lead, lithium and calcium

X.H. Zheng, D.G. Walmsley*

Department of Physics and Astronomy, Queen's University of Belfast, BT7 1NN, United Kingdom

A B S T R A C T

Applying the Heine–Abarenkov pseudopotential to aluminium and lead in both the superconducting and normal states, Carbotte and coworkers have set a challenging standard befitting the status of the classic BCS superconductor theory. Upholding the same standard and equipped with the technique of numerical inversion, we have extracted alternative pseudopotentials from experimental data with minimal prejudgement that might cloud the physics. The two potentials are broadly consistent in the superconducting state but distinctly different in the normal state. This is an urgent issue requiring confirmation or refutation in the context of the current search for high temperature conventional superconductivity.

1. Introduction

Recently in a remarkable congruence of theory and experiment, high temperature conventional superconductivity was predicted, discovered and explained in the sulfur hydride system under pressure [1–3]. The theory involved is usually known as Eliashberg–Nambu formalism, an advanced variant of the classic superconductor theory of Bardeen, Cooper and Schrieffer (BCS) [4]. We foresee rapid further advances, hopefully towards realising room temperature superconductivity, once the theory has been refined and verified to eliminate current uncertainties that compromise its predictive power.

In this process recognition should be given to Carbotte and coworkers who, in applying Eliashberg–Nambu formalism creatively at a very early stage of its development, set a standard that was, and still is, very challenging [5–10] They evaluated the electron–phonon interaction, responsible for both superconductivity and normal state electrical resistivity, quantitatively from first principles. They applied the Heine–Abarenkov pseudopotential, originally designed to reproduce atomic energy levels, to evaluating the electron–phonon spectral density, $\alpha^2F(\nu)$, for aluminium and lead in the superconducting state. As a careful control measure they applied the same pseudopotential to evaluate electrical resistivity, $\rho(T)$, for the same metals. They compared the results of their calculations with previous experimental measurement.

The work of Carbotte and coworkers is of both historical and current significance, not only because it was pioneering in the field, but also because it revealed problems that have remained unsolved till this day. It showed that, while calculated $\alpha^2F(\nu)$ appears to be reasonably accurate [7,8], agreement between calculated and experimental $\rho(T)$ is not good for example at T=297 K in the case of aluminium, and seriously worse in the case of lead [5]. Naturally we have to ask: are there better pseudopotentials to describe the electron–phonon interaction in the metals? We also have to ask: are the pseudopotentials consistent in the two states?

We wish to get to the bottom of the problem. In addition to confirming the results of Carbotte et al, we proceed from the point of view that a pseudopotential is a phenomenological and task-specific entity often with a narrow mandate. Therefore we no longer apply the Heine–Abarenkov pseudopotential that was designed for a purpose other than electron–phonon interaction evaluation. Instead we start from experimentally measured values of $\alpha^2F(\nu)$ and $\rho(T)$ and deduce the relevant pseudopotential through a procedure of inversion. We determine the potential numerically with an accuracy as high as possible, so that it is dictated entirely by the experimental data and underlying theories; uncertainties are thus reduced to a minimum. We compare our pseudopotential from inversion with the Heine–Abarenkov potential and find surprising differences. There are implications closely germane to the search for high temperature conventional superconductivity.

This article is arranged as follows: in Section 2 we briefly review the history of the application of the Heine–Abarenkov potential to describe the electron–phonon interaction, in Section 3 we explain the nature of the Heine–Abarenkov pseudopotential, in Sections 4 and 5 we consider applications of pseudopotentials in the superconducting and normal states, in Sections 6 and 7 we extract alternative pseudopotentials from aluminium and lead in the superconducting and normal states

* Corresponding author.
E-mail address: dg.walmsley@qub.ac.uk (D.G. Walmsley).

http://dx.doi.org/10.1016/j.ssc.2016.11.007
Received 27 September 2016; Accepted 6 November 2016
Available online 11 November 2016
0038-1098/

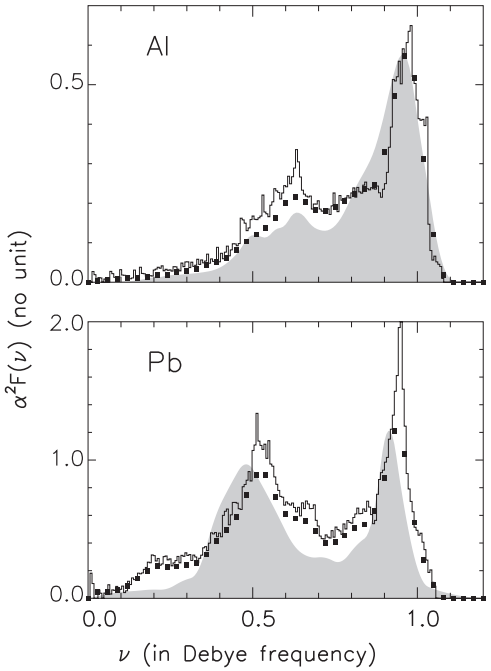

Fig. 1. Electron–phonon spectral densities in aluminium and lead in the superconducting state, grey silhouettes are from tunnelling measurement, histograms from the Heine–Abarenkov pseudopotentials and dark filled squares from alternative pseudopotentials.

respectively, in Section 8 we investigate lithium and calcium as two further examples, brief discussion and conclusions are presented in Sections 9 and 10.

2. Historical review

The Eliashberg–Nambu formalism quickly surpassed the original generic BCS theory and enabled McMillan to devise a procedure of inversion for individual materials that directly links $\alpha^2F(\nu)$ to data from experimental tunnelling conductance measurements [13]. Success of the McMillan procedure immediately led to an upsurge of further successful research activity, see [8] and references therein. The obvious next move was to evaluate $\alpha^2F(\nu)$ from first principles and at this stage difficulties started to emerge.

In 1968 Carbotte and Dynes [8] evaluated $\alpha^2F(\nu)$ for aluminium with the Heine–Abarenkov pseudopotential specified by Harrison [14]. In general their result, shown as the histogram in the upper part of Fig. 1 (evaluated in house), is in commendable agreement with the experimental result (grey silhouette).

In 1971 Leavens and Carbotte followed the approach of Bennett to reveal phonon anisotropy of $\alpha^2F(\nu)$ also with the Harrison pseudopotential [9,10]. This approach is perturbational, with a spherical Fermi surface and anisotropy due entirely to phonons. It starts from an isotropic $\alpha^2F(\nu)$ which, though claimed to be with some corrections, appears to be the same as that in [4].

In 1976 Leung et al. once more evaluated anisotropic $\alpha^2F(\nu)$ for aluminium, with the same Harrison potential but with a non-spherical Fermi surface. Values of $\alpha^2F(\nu)$ appear to have changed little [11].

In 1976 Tomlinson and Carbotte evaluated $\alpha^2F(\nu)$ for lead in the superconducting state [12]. The electron–phonon interaction was evaluated with a non-spherical Fermi surface, with the Heine–Abarenkov pseudopotential specified by Appapillai and Williams [15]. Agreement between theory and measurement was considered as "very good" [4], although the longitudinal numerical peak of $\alpha^2F(\nu)$ at 9 meV is more than 2 times as strong as that observed in the experimental tunnelling peak [4,7]. This excessive peak disappears in our evaluation, with the same pseudopotential, shown as the histogram in the lower part of Fig. 1.

When looking at Fig. 1 one can be forgiven for believing that all is well on the theory front. Application of the Heine–Abarenkov pseudopotential, specified by Harrison et al, appears to be just the right way forward to describe the electron–phonon interaction in metals. It is remarkable that Carbotte and coworkers did not stop here but carried on to investigate $\rho(T)$ of the metals that arises from the same electron–phonon interactions.

In 1968 Dynes and Carbotte [5] calculated $\rho(T)$ of some simple metals from first principles with the Harrison pseudopotentials [14]. In the abstract of the publication it is stated that good agreement is obtained with experiment for both absolute value and detailed variation with temperature. However in the text it was acknowledged that for aluminium the agreement is not particularly good at 297 K. It was also acknowledged that for lead deviations from experiment are more serious.

In 1973 Truant and Carbotte published further details of $\rho(T)$ calculation for aluminium, with two slightly different formulations to smooth out phonon anisotropy [6]. They show their results on a logarithmic scale that reveals detailed differences between the two formulations at low temperatures. We evaluate one of their formulations and present the outcome on a linear scale, see the grey line in the upper part in Fig. 2. The numerical and experimental $\rho(T)$ indeed deviate significantly at T=295 K as is remarked in [5].

In 1977 Tomlinson and Carbotte [12] evaluated $\rho(T)$ in lead with the Heine–Abarenkov pseudopotential specified by Appapillai and Williams [15]. They evaluated electron–phonon interactions at just 31 selected points of the Fermi surface. Their $\rho(T)$, shown graphically by Eiling and Schilling (filled dark squares in the lower part of Fig. 2) [16], indeed deviates seriously from experimental data as is acknowledged in [5]. The situation takes a turn for the worse when we evaluate the electron–phonon interaction over the entire Fermi surface, see the grey line in the lower part of Fig. 2.

With the startling contrast in performance of the Heine–Abarenkov pseudopotential between Figs. 1 and 2, we have to ask: do we have a consistent pseudopotential in both the normal and superconducting states?

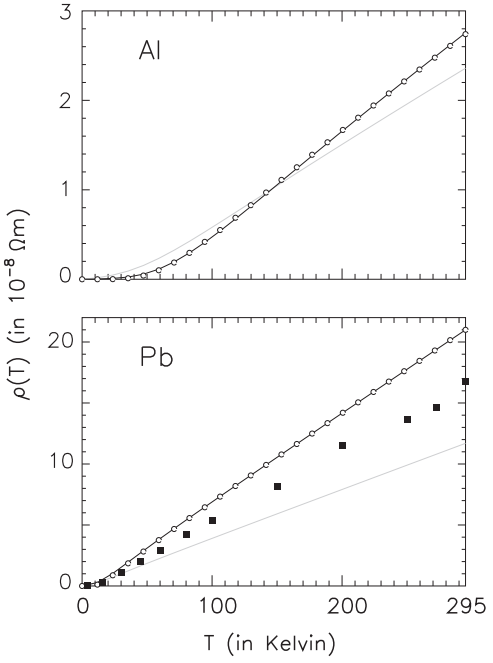

Fig. 2. Electrical resistivity of aluminium and lead in the normal state, open circles are experimental values, grey curves from Heine–Abarenkov pseudopotentials, solid squares from Tomlinson and Carbotte calculation [12] and dark curves from pseudopotentials optimised via inversion.

3. Heine–Abarenkov pseudopotential

In its original design the Heine–Abarenkov pseudopotential is of the following form:

$$V(\mathbf{r}) = \sum_{\ell} V_{\ell}(r) P_{\ell} \tag{1}$$

where $V_{\ell}(r)$ is the model potential, r the distance from the atom in real space,

$$P_{\ell} = \sum_{m=-\ell}^{\ell} |Y_{\ell}^{m}\rangle\langle Y_{\ell}^{m}| \tag{2}$$

the projection operator, with Y_{ℓ}^{m} being spherical harmonics, helping to identify a designated term from the many-electron wavefunction and then restoring the angular pattern of that term. The radial pattern of the term in question is a spherical Bessel function over a core range of r, where $V_{\ell}(r)$ is assumed to be constant with a value $-A_{\ell}$. By adjusting the value of A_{ℓ} it is possible to reproduce the energy level of the atomic valence electron with the angular pattern Y_{ℓ}^{m}. Usually three energy levels are reproduced [17,18].

Animalu and Heine [18] place Eq. (1) in the context of electron scattering and find the following matrix element:

$$V(q)S(\mathbf{q}) = \langle \mathbf{k} + \mathbf{q}|V(\mathbf{r})|\mathbf{k}\rangle \tag{3}$$

where $V(q)$ is known as the form factor and $S(\mathbf{q})$ a phase factor, $\mathbf{k}$ and $\mathbf{k} + \mathbf{q}$ mark the initial and end states of the electron respectively and $V(\mathbf{r})$ is defined in Eq. (1). We are reminded that in Eq. (1) the atom is assumed static. The electron is scattered because it encounters a potential well, not because the atom is vibrating. This process does not involve phonons and $\mathbf{q}$ in Eq. (3) has nothing to do with phonon momentum.

Numerical values of $V(q)$ in Eq. (3) are shown graphically (continuous curves) in Fig. 3 for aluminium and lead, data from [15]. Note that the range of q is extensive ($0 \le q \le 2k_F$ in a solid). Judging from its appearance $V(q)$ could have been the Fourier transform of some simple potential well in real space, but a very different story is told by the following formal inverse Fourier transform:

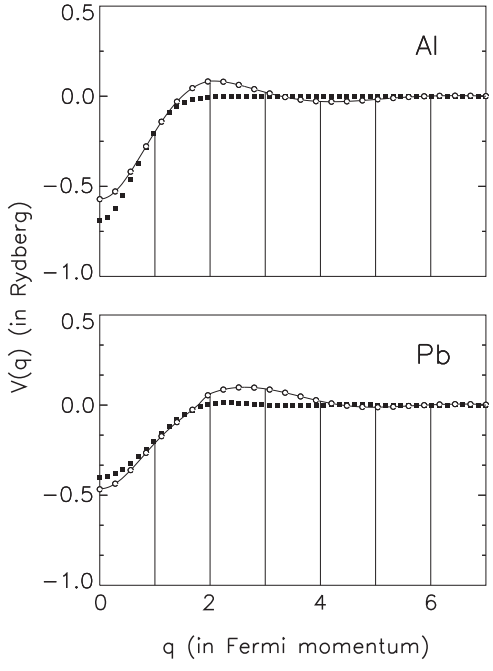

Fig. 3. Curves: form factors of the Heine–Abarenkov pseudopotentials in aluminium and lead; open circles: double Fourier transforms of Heine–Abarenkov pseudopotentials for numerical accuracy assurance; filled dark squares: alternative pseudopotentials from superconductivity inversion.

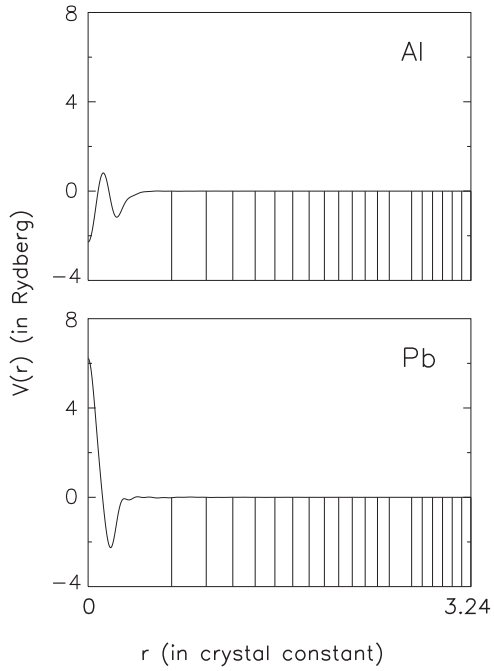

Fig. 4. Form factors of the Heine–Abarenkov pseudopotentials in aluminium and lead in real space. In a crystal, other atoms are arranged away from an atom in a serious of spherical shells, with increasing radii as indicated here for the fcc lattice by the vertical lines.

$$V(r) = \frac{3}{q_D^3} \int V(q) j_0(qr) q^2 dq \tag{4}$$

where q_D is the Debye momentum and j_0 a spherical Bessel function. We see from the upper part of Fig. 4 that, in real space, $V(r)$ for aluminium oscillates significantly over a range close to the atomic site. From the lower part of Fig. 4 we see that for lead $V(r)$ has, by contrast, a strong peak at the atomic site, hardly reminiscent of a screened Coulomb potential well.

With the following Fourier transform

$$V(q) = \frac{3}{r_0^3} \int V(r) j_0(qr) r^2 dr \tag{5}$$

we can recover $V(q)$ in Eq. (3) from $V(r)$, with r_0 being the radius of the Wigner–Seitz cell, for the purpose of numerical accuracy assurance. In Fig. 3 we use the open circles to present values of $V(q)$ from successive applications of Eqs. (4) and (5) (double Fourier transform). Apparently the numerical accuracy is adequate and the unusual features of $V(r)$ in Fig. 4, including significant oscillation and the strong peak towards r=0, are genuine.

4. Superconductivity

In the Eliashberg–Nambu formalism the strength of superconductivity is measured by the electron–phonon spectral density with the following definition:

$$\alpha^2 F(\nu) = \frac{1}{N} \sum_{\mathbf{q},\ell} \delta(\nu - \hbar\omega_{\ell}) \delta(\epsilon - \epsilon_F) |g_{\ell}(\mathbf{q})|^2 \tag{6}$$

where N is the number of atoms in a unit volume, $\mathbf{q}$ phonon vector momentum, ℓ identifies phonon polarisation, ω_{ℓ} phonon frequency, ϵ and ϵ_F electron and Fermi energy respectively and

$$g_{\ell}(\mathbf{q}) = \sqrt{\frac{\hbar}{2M\omega_{\ell}}}\, \mathbf{e}_{\ell} \cdot \langle \mathbf{k} + \mathbf{q}|\nabla V(\mathbf{r})|\mathbf{k}\rangle \tag{7}$$

is the matrix element for the electron–phonon interaction, with M being the mass of atom. In Eq. (7) the atomic potential is differentiated

with respect to real space variables, **r**, in order to access the effect of atomic displacement on an electron, and $\mathbf{e}_\ell$ arises from phonon polarisation [4].

We transform Eqs. (6) and (7) into a programmable version [19]. To this end we have to transform summation over **q** in Eq. (6) into integration over ω_ℓ. Therefore we have to evaluate $d\omega_\ell/dq$ from phonon data, the most laborious part of the numerical work. To start we have to find a sufficiently accurate relation between ω_ℓ and q (phonon dispersion). We assume that the Coulomb force between atoms depends only on the interatomic distance (central force model) and calibrate the force constants with neutron scattering data (Born–von Karman theory). The task is relatively straightforward for aluminium when, for sufficiently accurate dispersion, we are able to cut the interatomic force off beyond the 6th spherical shell formed by other atoms surrounding a given atom, see [19] for further details. For lead we have to calibrate the interatomic force over 20 atomic shells, see Fig. 4 for locations of the shells, see [20] for further details and an interesting story.

In addition we have to understand the implication of the term $d\omega_\ell/dq$ and evaluate it properly. Sometimes this term becomes vanishingly small, telling us that an extraordinarily large number of phonon states is accommodated within a small range of phonon frequencies. This may lead to a spectacular longitudinal peak of the phonon density of states if we simply differentiate the dispersion curve numerically. We devised a method to avoid this difficulty, see [19] for further details.

Equipped with the above numerical technique we evaluate $\alpha^2F(\nu)$ with Eqs. (6) and (7). We repeat the work of Carbotte and coworkers, with the same Heine–Abarenkov pseudopotentials, and find results consistent with theirs in the case of aluminium [10], see the upper part of Fig. 1. In the case of lead our $\alpha^2F(\nu)$ has a longitudinal peak of a reasonable height, in contrast to the spectacularly huge peak in [12], see the lower part of Fig. 1.

5. Electrical resistivity

Both superconductivity and normal state electrical resistivity arise from the electron–phonon interaction. Indeed in the normal state the strength of the electron–phonon interaction is measured by the transport spectral density with the following definition:

$$\alpha^2_{\rm tr}F(\nu) = \frac{1}{N}\sum_{\mathbf{q},\ell}\delta(\nu-\hbar\omega_\ell)\delta(\epsilon-\epsilon_F)\frac{\mathbf{k}\cdot\mathbf{q}}{\mathbf{k}\cdot\mathbf{k}}|g_\ell(\mathbf{q})|^2 \tag{8}$$

that is very similar to the superconductor spectral function, $\alpha^2F(\nu)$ in Eq. (6), including an identical matrix element, $g_\ell(\mathbf{q})$, for the electron–phonon interaction defined in Eq. (7). It goes with the following formula:

$$\frac{1}{\tau} = 4\pi\frac{k_BT}{\hbar}\int_0^\infty \frac{\alpha^2_{\rm tr}F(\nu)xdx}{(e^x-1)(1-e^{-x})} \tag{9}$$

for electron relaxation time in metals that leads through the Drude formula to $\rho(T)$, x = ν/k_BT [21] with k_B being the Boltzmann constant. Eq. (9) is different from, though it shares some common features with, the empirical Bloch–Glüneisen formula [22].

We repeat the work of Carbotte and coworkers in [6,7] with the same Heine–Abarenkov pseudopotentials. We apply the Bloch–Grüneisen formula with an appropriate characteristic temperature, T_ρ (=375 K in the case of aluminium), that is known to reproduce experimental $\rho(T)$ for each material with sufficiently high accuracy (small circles in the upper part of Fig. 2) [22]. We use the grey line to show the numerical $\rho(T)$ from Eqs. (8) and (9), pseudopotential from [15]. It is higher than the circles at low T, lower at the high T, and crossing over at $T \sim 140$ K. In [6] the crossing point is at $T \sim 80$ K, reasonably close to ours considering that the curves of $\rho(T)$ in both cases are largely straight with similar orientations.

In the lower part of Fig. 2 we also use small circles to present $\rho(T)$ for lead from the Bloch–Grüneisen formula, $T_\rho = 86$ K [22]. The theoretical grey line from Eq. (9), pseudopotential from [15], is much lower than the circles. It also is considerably lower than the filled dark squares for the numerical $\rho(T)$ in [7], arising from the considered approach of the authors in evaluating Eq. (8): they selected just 31 values of **q** to evaluate Eq. (8) and carefully avoided places where the Fermi surface does not exist [7]. It is not clear whether or not they chose the same 31 values of **q** when they evaluated $\alpha^2F(\nu)$ in lead in the superconductive state in [12].

6. Superconductivity inversion

We evaluate Eqs. (6) and (7) with as little prejudgement as possible. In the case of aluminium we start with the following Gaussian potential:

$$V(r) = \delta V \exp\left[-\left(\frac{r}{r_1}\right)^2\right] \tag{10}$$

where δV and r_1 are parameters defining the depth and width of the potential well respectively to model the core charge of a lattice atom subject to screening. It leads through Eqs. (6) and (7) to values of $\alpha^2F(\nu)$. We can adjust the values of δV and r_1 in Eq. (10) to minimise the difference between theoretical and experimental data of tunnelling conductance [19], that is we are seeking the potential via a procedure of inversion with no physics other than what is implied by Eqs. (6) and (7).

In the case of aluminium the Gaussian potential in Eq. (10) is specified by $\delta V = -0.966$ Ry and $r_1 = 0.318a$, with a being the crystal constant. It leads via Eq. (5) to $V(q)$ in reciprocal space, with a maximum depth of 0.691 Ry, see the filled dark squares in the upper part of Figs. 3 and 5. In the upper part of Fig. 6 we also show $V(r)$ for aluminium from Eq. (10) as filled dark squares.

In the upper part of Fig. 3 the Gaussian potential in reciprocal space (filled dark squares) matches the Heine–Abarenkov pseudopotential for aluminium (curve and open circles) closely. This explains why, in the upper part of Fig. 1, values of $\alpha^2F(\nu)$ from inversion (filled squares) match those from the Heine–Abarenkov potential (histogram) so closely. On the other hand, in the upper part of Fig. 6, the Gaussian

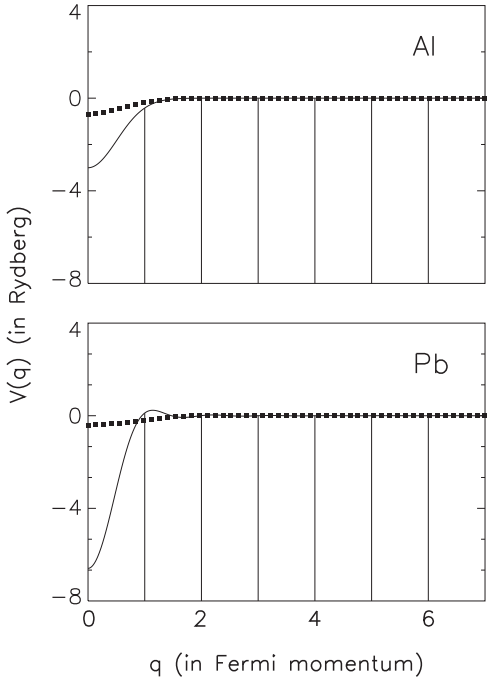

Fig. 5. Alternative pseudopotentials in reciprocal space for aluminium (upper) and lead (lower) in the normal (curves) and superconducting (filled squares) states.

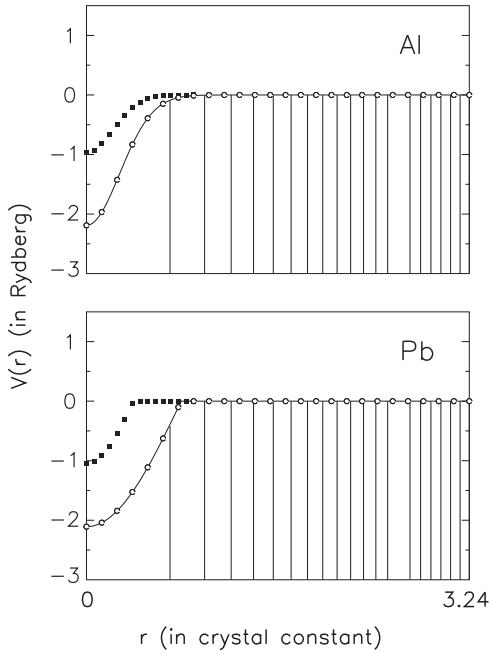

Fig. 6. Upper: alternative pseudopotentials in real space for aluminium (upper) and lead (lower) in the normal (curves) and superconducting (filled squares) states, open circles are from double Fourier transform for numerical accuracy assurance, vertical lines mark radii of atomic shells.

potential in real space (filled squares) is a world apart from the oscillating Heine–Abarenkov potential in real space in the upper part of Fig. 4. Apparently it is chance coincidence that $V(r)$ from Eqs. (1) and (10), so vastly different from each other in both values and physics, lead to similar $V(q)$ in reciprocal space.

For completeness we note that in a previous publication [19] we found $V(r)$ in aluminium in the superconducting state via a slightly different inversion procedure: we sought $V(q)$ in reciprocal space, free to vary over the range $0 \le q \le 2k_F$, and then converted it via Eq. (4) into a potential well in real space, with a maximum depth slightly deeper than 1 in Fermi energy, compared with the current depth ~1.13 in Fermi energy.

Next we turn our attention to lead. In some instances, such as here, we have to replace Eq. (10) with the following muffin–tin potential:

$$V(r) = \delta V \cos\left(\frac{\pi r}{2r_1}\right) \tag{11}$$

where $r r_1$, otherwise $V(r) = 0$. For lead in the superconducting state we find an optimal fit with $\delta V = -1.052$ Ry and $r_1 = 0.398a$, as seen in the continuous curve in the lower part of Fig. 6. In reciprocal space $V(q)$ has a maximum depth 0.402 Ry, as seen in the lower part of Fig. 5. Once more our alternative (muffin-tin) potential is close to the Heine–Abarenkov potential in reciprocal space, see the lower part of Fig. 3, but differs from it significantly in real space, see the lower part of Figs. 4 and 6. In a previous publication [19] we also found via inversion an alternative pseudopotential for lead in the superconducting state, with $V(r)$ having a maximum depth slightly greater than 1.2, compared with the current depth 1.53, both in units of Fermi energy.

7. Resistivity inversion

Now we evaluate Eqs. (7) and (8) for aluminium with the alternative pseudopotentials, adjusted to fit the theoretical $\rho(T)$, $0 \le T \le 295$ K, to the experimental data. We find $\delta V = -2.193$ Ry and $r_1 = 0.395a$ in Eq. (10), giving the numerical $V(r)$ in real space, shown as the curve and small open circles in the upper part of Fig. 6, and $V(q)$ in reciprocal space, shown as the curve in the upper part of Fig. 5. These lead to numerical values of $\rho(T)$ (dark curve) in the upper part of Fig. 2, on average differing from experimental values (open circles) by just 0.90% compared with ρ at 295 K.

In a previous publication [21] we first applied the Gaussian potential in Eq. (10) to pilot inversion ($\delta V = -2.414$ in Fermi energy and $r_1 = 0.381a$) and then refined the potential on 26 nodes between r=0 and $2.45a$ (radius of the 12th atomic shell), compared with the current values $\delta V = -2.193$ in Fermi energy and $r_1 = 0.395a$. Average deviation between numerical and experimental $\rho(T)$ was slightly better (0.18% compared with ρ at 295 K).

In the case of lead in the normal state we find $\delta V = -2.108$ Ry and $r_1 = 0.802a$ in Eq. (11), $V(r)$ shown in the lower part of Fig. 6 (curve and open circles), $V(q)$ shown in the lower part of Fig. 5 (solid curve), on average numerical $\rho(T)$ differs from experimental values by just 0.14% compared with ρ at 295 K. In previous pilot inversion [21] we had $\delta V = -3.61$ in Fermi energy and $r_1 = 0.497a$, compared with the current values $\delta V = -3.06$ in Fermi energy and $r_1 = 0.802a$, with spectacularly small deviation between theory and experiment (0.03% relative to ρ at 295 K after potential refinement).

8. Further examples

In general the Heine–Abarenkov pseudopotential does not describe the electron–phonon interaction in metals in the normal state sufficiently accurately. We briefly consider two other examples. In the upper part of Fig. 7 we use small circles to show $\rho(T)$ in lithium (bcc) from the Bloch–Grüneisen formula, $T_\rho = 381$ K from fitting to data in [23] (363 K in [22]). With $\delta V = -0.372$ Ry and $r_1 = 0.831a$ in Eq. (11) we find the dark line crossing the open circles, with an average deviation 0.51% between theoretical and measured values between T=0 and 295 K compared with ρ at 295 K. The grey line, from $V(q)$ tabulated by Appapillai [15], is significantly higher than the circles. Though not illustrated here, we have evaluated $\rho(T)$ for sodium (bcc) with the Appapillai $V(q)$ [15] and find that it too is significantly higher than the experimental values.

In the lower part of Fig. 7 we use small open circles to show $\rho(T)$ in calcium (fcc) from the Bloch–Grüneisen formula, $T_\rho = 150$ K [22]. With $\delta V = -0.394$ Ry and $r_1 = 0.719a$ in Eq. (11) we find the dark line

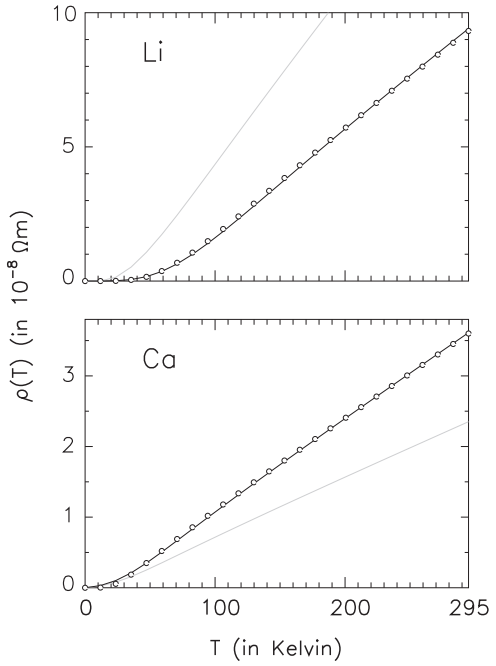

Fig. 7. Electrical resistivity of Li and Ca in the normal state, open circles are experimental values, grey lines are calculated from $V(q)$ tabulated by Appapillai, dark lines are calculated from alternative muffin-tin pseudopotentials.

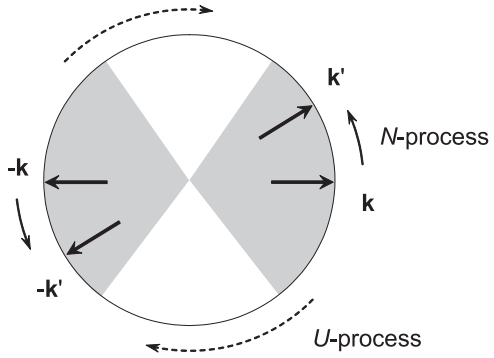

Fig. 8. Schematic of a spherical Fermi surface and a pair of electrons with initial states $\mathbf{k}$ and $-\mathbf{k}$. The end states, $\mathbf{k}'$ and $-\mathbf{k}'$, can be accessed via both normal (N) and umklapp (U) scattering, with different pair occupation probabilities, causing a dilemma.

crossing the open circles, with an average deviation between theoretical and measured values of 0.39% between T=0 and 295 K compared with ρ at 295 K. The grey line is from $V(q)$ tabulated by Appapillai [15]. It deviates significantly from the experimental values of $\rho(T)$, similar to the grey line for lead (fcc) in Fig. 2.

9. Discussion

A genuine issue often leaves a trace in the literature before it actually attracts seriously focussed attention. The issue of inconsistent pseudopotentials in the normal and superconducting states, shown clearly in Figs. 5 and 6, has been reported sporadically by a considerable number of authors, see [20] for a brief historical review, in addition to the review in Section 2 here.

Previously a single potential for a Coulomb effect, such as the Heine–Abarenkov pseudopotential, was often substituted into Eq. (7) which was then applied to Eqs. (6) and (8) for the superconducting and normal states respectively. This practice has masked the seriousness of the difficulty, because in Eq. (8) the factor $\mathbf{k}\cdot\mathbf{q}$ is small around the centre of the potential well (where $q \ll k_F$) in reciprocal space. The well has to be deepened considerably in order to mend the seemingly insignificant difference between the numerical and experimental $\rho(T)$ in say the upper part of Fig. 2. Fig. 5 tells us how much the potential well has to be deepened in aluminium and lead in the normal state. See [21] to appreciate how much it has to be deepened in niobium and tantalum.

How does the above issue arise? In short: normal and umklapp scattering may compete for the same destination pair states. In normal electron–phonon scattering the end states from $\mathbf{k}$ are restricted to the grey wedge on the right (angle = 78.1°, 60.0°, 51.8°, … when valency = 1, 2, 3, …). They can never reach the wedge on the left. End states of umklapp scattering, in contrast, do cover the left wedge [24] and this causes problems.

Specifically in Fig. 8 in normal scattering an electron in a Cooper pair experiences a transition from $\mathbf{k}$ to $\mathbf{k}'$ (other electron from $-\mathbf{k}$ to $-\mathbf{k}'$ by symmetry) giving a pair occupation probability $h(\mathbf{k}') = h(-\mathbf{k}')$. In umklapp scattering the transition is from $\mathbf{k}$ to $-\mathbf{k}'$ (other electron from $-\mathbf{k}$ to $\mathbf{k}'$ by symmetry) giving another distinct pair occupation probability $u(\mathbf{k}') = u(-\mathbf{k}')$. In general $h(\mathbf{k}') \neq u(\mathbf{k}')$ because of the different phonons (solid and dashed arrows) involved in the N and U-processes. Should we adopt $h(\mathbf{k}')$ or should we adopt $u(\mathbf{k}')$? That is the dilemma underlying the current issue [25].

In the original BCS theory the above dilemma manifests itself through a ground state electron wavefunction that cannot be normalised [25]. Keeping this in mind we have devised an electron-pairing rule in the BCS theory that allows a consistent pseudopotential to describe the electron–phonon interaction in both the normal and superconducting states [21].

10. Conclusions

The work of Carbotte and coworkers has cast a long shadow over the field of superconductivity. Following their success in using the Heine–Abarenkov pseudopotential to describe the electron–phonon interaction in aluminium and lead in the superconducting state, they carried on to investigate whether the same potentials were applicable in the normal state. Here, they were the first, among many other authors, to encounter a difficulty in the BCS theory. Equipped with alternative better pseudopotentials obtained through numerical inversion, we show that the problem is serious but can be resolved through the introduction of a modified electron pairing rule in the BCS theory. Drozdov et al. have very helpfully measured both superconductivity and normal state electrical resistivity in sulfur hydride and sulfur deuteride [2]. Do we have a consistent pseudopotential to explain their results in the two states? This is an important question with its roots in the early work of Carbotte and coworkers and requiring detailed computation using for example the method of numerical inversion for its answer.

References

[1] Y. Li, J. Hao, H. Liu, Y. Ma, J. Chem. Phys. 140 (2014) 174712.
[2] A.P. Drozdov, M.I. Eremets, I.A. Troyan, V. Ksenotov, S.I. Shylin, Nature 525 (2015) 73.
[3] R. Akashi, M. Kawamura, S. Tsuneyuki, Y. Nomura, R. Arita, Phys. Rev. B 91 (2015) 224513.
[4] J.P. Carbotte, Rev. Mod. Phys. 62 (1990) 1027.
[5] R.C. Dynes, J.R. Carbotte, Phys. Rev. 175 (1968) 913.
[6] P.T. Truant, J.P. Carbotte, Can. J. Phys. 52 (1974) 618.
[7] P.G. Tomlinson, J.P. Carbotte, Can. J. Phys. 55 (1977) 751.
[8] J.P. Carbotte, R.C. Dynes, Phys. Rev. 172 (1968) 476.
[9] C.R. Leavens, J.P. Carbotte, Solid State Commun. 9 (1971) 75.
[10] C.R. Leavens, J.P. Carbotte, Ann. Phys. 70 (1972) 338.
[11] H.K. Leung, J.P. Carbotte, C.R. Leavens, J. Low Temp. Phys. 24 (1976) 25.
[12] P.G. Tomlinson, J.P. Carbotte, Phys. Rev. B 13 (1976) 4738.
[13] W.L. McMillan, Phys. Rev. 167 (1968) 331.
[14] W.A. Harrison, Pseudopotentials in the theory of metals, Benjamin, New York, 1966.
[15] M. Appapillai, A.R. Williams, J. Phys. F: Met. Phys. 3 (1973) 759.
[16] A. Eiling, J.S. Schilling, J. Phys. F: Met. Phys. 11 (1981) 623.
[17] I.V. Abarenkov, V. Heine, Philos. Mag. 12 (1965) 529.
[18] A.O.E. Animalu, V. Heine, Philos. Mag. 12 (1965) 1249.
[19] X.H. Zheng, D.G. Walmsley, J. Low Temp. Phys. 166 (2012) 279.
[20] X.H. Zheng, D.G. Walmsley, Solid State Commun. 237–238 (2016) 42.
[21] X.H. Zheng, D.G. Walmsley, J. Low Temp. Phys. 173 (2013) 120.
[22] J.M. Ziman, Electrons and Phonons, Clarendon, Oxford, 2001.
[23] T.C. Chi, J. Phys. Chem. Ref. Data 8 (1979) 339–438.
[24] J.P. Carbotte, R.C. Dynes, Phys. Rev. 172 (1968) 476.
[25] X.H. Zheng, D.G. Walmsley, Phys. Scr. 89 (2014) 095803.